Werk

Jahr: 1986
Kollektion: fid.geo
Signatur: 8 Z NAT 2148:60
Digitalisiert: Niedersächsische Staats- und Universitätsbibliothek Göttingen
Werk Id: PPN1015067948_0060
PURL: http://resolver.sub.uni-goettingen.de/purl?PPN1015067948_0060

LOG Id: LOG_0014
LOG Titel: Fast plane-wave and single-shot migration by Fourier transform
LOG Typ: article

Übergeordnetes Werk

Werk Id: PPN1015067948
PURL: http://resolver.sub.uni-goettingen.de/purl?PPN1015067948
OPAC: http://opac.sub.uni-goettingen.de/DB=1/PPN?PPN=1015067948

Contact

Niedersächsische Staats- und Universitätsbibliothek Göttingen
Georg-August-Universität Göttingen
Platz der Göttinger Sieben 1
37073 Göttingen
Germany
Email: gdz@sub.uni-goettingen.de

J Geophys (1986) 60:19–27

Journal of Geophysics

Fast plane-wave and single-shot migration by Fourier transform

Paul Temme[1] * **and Gerhard Müller**[2]

[1] Department of Geology and Geophysics, University of Utah, Salt Lake City, UT 84112, USA
[2] Institute of Meteorology and Geophysics, Feldbergstrasse 47, D-6000 Frankfurt/M., Federal Republic of Germany

Abstract. A method is presented by which plane-wave and single-shot migration can be performed very fast through Fourier transformation. The technique is similar to Stolt's (1978) migration procedure for CMP data; however, it is based on plane-wave and single-shot sections as input data. For the reconstruction of the subsurface structure, the appropriate imaging conditions are used (Temme, 1984), and the velocity is assumed to be constant. Plane-wave migration can be performed exactly, single-shot migration is exact only along a ray leaving the shot with a specified direction and close to it. The theory is tested on synthetic seismograms for a synclinal structure and a set of horizontal reflector elements separated by gaps. The proposed method requires mapping of the frequency-wavenumber spectrum corresponding to the observations, on to the two-dimensional wavenumber spectrum corresponding to the migrated section. The latter spectrum has to be sampled with sufficient detail, otherwise pronounced aliasing effects will appear in the migrated section. A time-saving alternative is to apply a smoothing phase-shift operation to the frequency-wavenumber spectrum and to remove the phase shift from the spectrum of the migrated section.

Key words: Prestack frequency-wavenumber migration – Directional migration – Computational aspects

Introduction

Modern migration techniques employ the scalar wave equation in order to reconstruct the subsurface structure from seismic wave fields measured at the earth's surface. Usually, common midpoint sections (CMP sections) are used as input data in standard migration. The exploding reflector model is employed (Loewenthal et al., 1976), i.e. the CMP wave field is downward continued in a first step to different depth levels by solving the wave equation using half the material velocity. In a second step, the migrated depth section $M(x, z)$ is constructed by taking the downward-continued wave field $U(x, z, t)$ for each depth level z at the imaging time $t_I = 0$:

$$M(x, z) = U(x, z, t_I = 0).$$

Instead of using a CMP section as input, plane-wave sections and single-shot sections can be used for the reconstruction of subsurface structures. A plane-wave section is the plane-wave response of an arbitrarily shaped structure due to an incident plane wave with a fixed angle of propagation. A single-shot section represents the reflected wave field at the earth's surface for point- or line-source excitation. In common seismic surveys, several single-shot sections are recorded by shifting the shotpoint-geophone configuration across the structure being investigated. These single-shot wave fields represent the data base for standard CMP stacking (Mayne, 1962). On the other hand, single-shot sections can also be used for synthesizing plane-wave sections by slant stacking (Schultz and Claerbout, 1978; Treitel et al., 1982). Plane-wave and single-shot sections represent physical wave fields that can be measured in a realistic physical experiment. Therefore, one can expect to be able to determine the reflection coefficients of the structure. This is more difficult in the case of CMP migration, which starts from a manipulated (and, in that sence, nonphysical) wave field (Temme, 1984).

The role plane-wave and single-shot migration could play in the reconstruction of subsurface structures is currently restricted to the detailed investigation of selected reflecting elements. Because of the finite geophone spread that is used to record the reflections, only segments of the structure can be seen. In order to obtain the total subsurface structure, as in the case of CMP migration, many single-shot sections with different shotpoint locations or many plane-wave sections with different angles of incidence have to be migrated. From a practical point of view this is only attractive if rapid algorithms performing single-shot and plane-wave migration are available.

The fastest migration algorithms have been formulated in the frequency-wavenumber domain. Gazdag (1978) presented the phase-shift method for CMP sections, where the Fourier-transformed wave field at the surface is downward continued to each desired depth level z using an appropriate z-dependent phase-shift operator. The migrated section results from subsequently evaluating the downward-continued wave field at time $t = 0$. At each depth level the inverse

* *New address:* Institute of Planetology, University of Münster, Corrensstraße 24, D-4400 Münster, Federal Republic of Germany

Offprint requests to: P. Temme

Fourier transform from frequency to time is a simple summation of all frequency components. Finally, one depth level of the migrated section is obtained by a one-dimensional inverse Fourier transform over the horizontal wavenumber k_x. Stolt (1978) presented another fast algorithm of frequency-wavenumber migration. In his method the total depth structure $M(x, z)$ is calculated from the Fourier-transformed CMP section in one step. The frequency-wavenumber integral is transformed to a Fourier integral over k_x and the vertical wavenumber k_z using the substitution $k_z=\left(\frac{\omega^2}{c^2}-k_x^2\right)^{\frac{1}{2}}$, where c is half the wave velocity. The downward-continued wave field is only evaluated at time $t=0$. This Fourier integral can be calculated by an inverse two-dimensional Fast Fourier Transform (FFT) and results in the total migrated depth section.

Frequency-wavenumber migration deals with velocity variation only in an approximate way. Gazdag's phase-shift method allows for depth-dependent velocity only. For laterally varying velocity, Gazdag and Squazzero (1984) proposed an interpolation method. Stolt's method has the disadvantage of not allowing any velocity variation. In order to alleviate this difficulty he proposed a stretching of the time axis of each zero-offset seismogram, incorporating the root mean square velocity (Stolt, 1978: Eq. 75; Claerbout, 1985: p. 276). The transformed wave field looks more like it had come from a constant velocity structure. In spite of the weakness in dealing with varying velocity, the frequency-wavenumber migration is widely used in industrial practice.

In this paper a migration algorithm, which is similar to Stolt's method but formulated for plane-wave and single-shot sections will be presented. In order to deal with non-CMP input data, modified imaging conditions for the construction of the migrated section have to be used. The imaging conditions for plane-wave and single-shot sections have been described by Temme (1984). They are based on the principle that reflectors exist at those points (x, z) within the structure where the reflected wave is time coincident with the downgoing wave. If we assume the velocity to be constant, the imaging conditions can be expressed analytically. In the plane-wave case we use

$$M(x, z)=U\left(x, z, t_I=\frac{x}{v}\sin\phi+\frac{z}{v}\cos\phi\right). \tag{1}$$

For single-shot sections we use

$$M(x, z)=U\left(x, z, t_I=\frac{(x^2+z^2)^{\frac{1}{2}}}{v}\right). \tag{2}$$

$M(x, z)$ represents the migrated depth section, U is the downward-continued reflected wave field at depth level z. t_I in Eq. (1) represents the arrival time of the downgoing plane wave measured from the surface point at $x=0$, where the plane wave passes at time $t=0$, to the reflection point at (x, z). The angle ϕ is the propagation angle of the plane wave with respect to the z axis. t_I in Eq. (2) is the arrival time of the downgoing cylindrical wave (2D case), taken from the shotpoint location at $(x=0, z=0)$ to the reflector at (x, z).

In the next section we will present the theory of plane-wave and single-shot migration in the Fourier domain. A discussion of computational aspects of the method and how aliasing can be avoided is included in a subsequent section. Finally, the method is tested on synthetic seismograms for simple subsurface structures: a synclinal structure and a set of horizontal reflectors with gaps.

Theory

Plane-wave migration

$U(x, z=0, t)$ represents the reflected scalar wave field, which is known at the earth's surface; the depth coordinate is positive downwards. In order to calculate the reflected wave field at a deeper level z, we use the scalar wave equation. Its solution will be given in the frequency-wavenumber domain, where the wave equation reads

$$\frac{d^2\bar{U}}{dz^2}+\left(\frac{\omega^2}{v^2}-k_x^2\right)\bar{U}=0. \tag{3}$$

$\bar{U}$ represents the Fourier-transformed reflected wave field; v is the constant material velocity. The following correspondences have been used:

$$\bar{U}(k_x, z, \omega)=\int_{-\infty}^{\infty}\int_{-\infty}^{\infty}U(x, z, t)\,e^{-i(\omega t+k_x x)}\,dt\,dx$$

$$U(x, z, t)=\frac{1}{4\pi^2}\int_{-\infty}^{\infty}\int_{-\infty}^{\infty}\bar{U}(k_x, z, \omega)\,e^{i(\omega t+k_x x)}\,d\omega\,dk_x. \tag{4}$$

The general solution of Eq. (3) is

$$\bar{U}(k_x, z, \omega)=Ce^{i\left(\frac{\omega^2}{v^2}-k_x^2\right)^{\frac{1}{2}}z}+De^{-i\left(\frac{\omega^2}{v^2}-k_x^2\right)^{\frac{1}{2}}z}.$$

For reasons of simplicity, we are only dealing with positive frequencies ω. Thus, the arguments of the exponential functions have only one sign. The first term with coefficient C represents waves travelling upwards in the negative z direction. The second term with the coefficient D represents waves travelling downwards. We are only interested in the downward continuation of upgoing reflected waves. For this reason, we choose $D=0$. C can be determined from the boundary condition for $z=0$: $C=\bar{U}(k_x, 0, \omega)$. Finally, we obtain the downward-continued wave field at level z from Eq. (4):

$$U(x, z, t)=\frac{1}{4\pi^2}\int_{-\infty}^{\infty}\int_{-\infty}^{\infty}\bar{U}(k_x, 0, \omega)\cdot e^{i\left[\omega t+k_x x+\left(\frac{\omega^2}{v^2}-k_x^2\right)^{\frac{1}{2}}z\right]}\,d\omega\,dk_x. \tag{5}$$

The migrated section $M(x, z)$ can be calculated by applying the imaging condition for plane waves, Eq. (1):

$$M(x, z)=\frac{1}{4\pi^2}\int_{-\infty}^{\infty}\int_{-\infty}^{\infty}\bar{U}(k_x, 0, \omega)\cdot e^{i\left\{\left(\frac{\omega}{v}\sin\phi+k_x\right)x+\left[\left(\frac{\omega^2}{v^2}-k_x^2\right)^{\frac{1}{2}}+\frac{\omega}{v}\cos\phi\right]z\right\}}\,d\omega\,dk_x. \tag{6}$$

The calculation of the depth section $M(x, z)$ using Eq. (6) is cumbersome because the frequency-wavenumber integral has to be solved for each depth level z. The total depth section can be calculated more efficiently by rewriting Eq. (6) as a Fourier integral, which can be computed very fast by using the FFT. This is achieved by introducing new variables A and B into (6):

$$A(\omega, k_x)=\frac{\omega}{v}\sin\phi+k_x \tag{7}$$

$$B(\omega, k_x)=\frac{\omega}{v}\cos\phi+\left(\frac{\omega^2}{v^2}-k_x^2\right)^{\frac{1}{2}}. \tag{8}$$

Equation (6) transforms into the Fourier integral

$$M(x, z)=\frac{1}{4\pi^2}\int_{-\infty}^{\infty}\int_{-\infty}^{\infty}\bar{U}[k_x(A, B), 0, \omega(A, B)] \cdot\left|\frac{\partial(\omega, k_x)}{\partial(A, B)}\right| e^{i(Ax+Bz)}\,dA\,dB, \tag{9}$$

from which we recognize A and B as new wavenumbers with respect to x and z. The Jacobian in Eq. (9) is

$$\frac{\partial(\omega, k_x)}{\partial(A, B)}=\frac{\partial\omega}{\partial A}\frac{\partial k_x}{\partial B}-\frac{\partial\omega}{\partial B}\frac{\partial k_x}{\partial A}.$$

Solving Eqs. (7) and (8) for k_x and ω, we obtain:

$$k_x(A, B)=\frac{(A^2-B^2)\sin\phi+2AB\cos\phi}{2(A\sin\phi+B\cos\phi)} \tag{10}$$

$$\omega(A, B)=\frac{v(A^2+B^2)}{2(A\sin\phi+B\cos\phi)}. \tag{11}$$

Calculating the Jacobian from these expressions and inserting into Eq. (9), we have the migrated section

$$M(x, z)=\frac{1}{4\pi^2}\int_{-\infty}^{\infty}\int_{-\infty}^{\infty}\bar{M}(A, B)\,e^{i(Ax+Bz)}\,dA\,dB \tag{12}$$

with the Fourier transform

$$\bar{M}(A, B)=\bar{U}[k_x(A, B), 0, \omega(A, B)] \cdot\left|\frac{v(A^2-B^2)\cos\phi-2AB\sin\phi}{2(A\sin\phi+B\cos\phi)^2}\right|. \tag{13}$$

Equation (12), together with Eqs. (13), (10) and (11), is the final solution which can be used to calculate the migrated section in one step with the aid of the FFT. Before we discuss some computational aspects of Eqs. (12) and (13), we will first derive the migration algorithm of single-shot sections.

Single-shot migration

In the case of single-shot migration, the imaging condition Eq. (2) has to be applied to Eq. (5). A problem arises from the nonlinear dependence of $t_I=\frac{(x^2+z^2)^{\frac{1}{2}}}{v}$ on x and z. t_I has to be approximated by a linear expression, which can be found by expansion into a Taylor series about (x_0, z_0) and neglecting higher-order terms:

$$t_I\approx\frac{(x_0^2+z_0^2)^{\frac{1}{2}}}{v}+\frac{1}{v(x_0^2+z_0^2)^{\frac{1}{2}}}[x_0(x-x_0)+z_0(z-z_0)]$$

$$=\frac{1}{v}\left(\frac{x_0}{R_0}x+\frac{z_0}{R_0}Z\right)$$

$$t_I\approx\frac{\sin\phi}{v}x+\frac{\cos\phi}{v}z. \tag{14}$$

$R_0=(x_0^2+z_0^2)^{\frac{1}{2}}$ is the distance from the shotpoint at ($x=0, z=0$) to the reflection point (x_0, z_0), and ϕ is the angle between the ray from shotpoint to reflection point and the z axis. From Eq. (14) we realize that the approximation of t_I does not depend on (x_0, z_0), but only on the angle ϕ. The imaging condition (14) for single-shot migration is exact for all points on the ray leaving the shotpoint under the angle ϕ, but errors are introduced away from this ray. Hence, single-shot migration with Eq. (14) can be considered as *directional sounding* of the subsurface: reconstruction will be correct for the direction ϕ and directions close to it, but deviations will develop for directions significantly different from ϕ.

The single-shot imaging condition (14) has the same form as the plane-wave imaging condition Eq. (1). Therefore, the same program coding as in the case of plane-wave migration can be used.

Computational aspects

In this section a few computational aspects of solving Eqs. (12) and (13) will be discussed. Figure 1 shows the transformation of $\bar{U}(k_x, 0, \omega)$ from the $\omega-k_x$ domain to the newly introduced $A-B$ wavenumber domain. Homogeneous waves, which we will consider here only, correspond to the shaded triangles shown in the left panel where $\left|\frac{\omega}{v}\right|\geqq|k_x|$. Elsewhere, $\bar{U}(k_x, 0, \omega)$ is equal to zero. By transforming the $\omega-k_x$ domain to the $A-B$ domain, lines of constant frequencies ω are imaged on to circles with centres located at $A=\frac{\omega}{v}\sin\phi$ and $B=\frac{\omega}{v}\cos\phi$. The horizontal and vertical Nyquist wavenumbers A_N and B_N have to meet the following conditions:

$$A_N=\frac{\pi}{\Delta x}\geqq\frac{\omega_N}{v}(1+\sin|\phi|), \tag{15a}$$

$$B_N=\frac{\pi}{\Delta z}\geqq\frac{\omega_N}{v}(1+\cos\phi). \tag{15b}$$

From these expressions follow the sampling intervals of the migrated section $M(x, z)$:

$$\Delta x\leqq\frac{v\Delta t}{1+\sin|\phi|}, \tag{16a}$$

$$\Delta z\leqq\frac{v\Delta t}{1+\cos\phi}. \tag{16b}$$

Here the circular Nyquist frequency $\omega_N=\frac{\pi}{\Delta t}$ has been used, where Δt is the time interval of the reflected wave field. The sampling intervals in the $A-B$ domain are

$$\Delta A=\frac{2\pi}{X}, \quad \Delta B=\frac{2\pi}{Z}, \tag{17}$$

where X is the length and Z the depth of the migrated section. X is usually assumed to be identical with the length L of the geophone array measuring the reflected wave field at $z=0$; this implies that $\Delta A=\Delta k_x$. For Z, a reasonable estimate has to be made. A possible choice is $Z=vT$, where T is the duration of the seismograms, representing the reflected wave field. The number of grid points in the $A-B$ domain (and in the $x-z$ domain) is determined by the in-

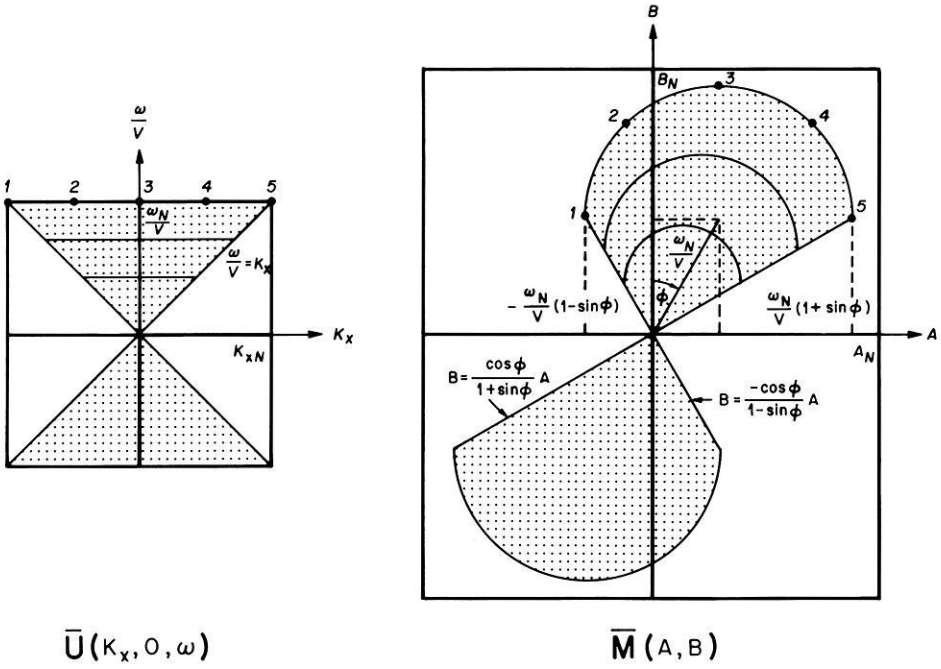

Fig. 1. Transformation of the Fourier-transformed reflected wave field $\bar{U}(k_x, 0, \omega)$ from the $k_x-\omega$ domain to the $A-B$ wavenumber domain. $\bar{M}(A, B)$ is the Fourier-transformed migrated section. Lines of constant frequency are mapped on to circles with centres at $A=\frac{\omega}{v}\sin\phi$ and $B=\frac{\omega}{v}\cos\phi$. A_N is the horizontal and B_N is the vertical Nyquist wavenumber. k_{xN} is the original horizontal Nyquist wavenumber and ω_N the temporal Nyquist frequency

tegers

$$LA=\frac{X}{\Delta x}, \qquad LB=\frac{Z}{\Delta z}. \tag{18}$$

With Eqs. (15)–(18) the grid on which the Fourier transform $\bar{M}(A, B)$ of the migrated section, Eq. (13), has to be calculated is known. $\bar{M}(A, B)$ is nonzero only in the shaded area of the right panel of Fig. 1, and the computation can be restricted to $B \geqq 0$. Inverse Fourier transformation of $\bar{M}(A, B)$ [and also calculation of $\bar{U}(k_x, 0, \omega)$] in the examples of this paper was performed with a FFT program written by Terefe (1985).

The computation of $\bar{M}(A, B)$ requires interpolation of $\bar{U}(k_x, 0, \omega)$, since the points in the $k_x-\omega$ domain, corresponding to the equidistant gridpoints in the $A-B$ domain according to Eqs. (10) and (11), will usually not fall on the gridpoints in which $\bar{U}(k_x, 0, \omega)$ is known. The two-dimensional sinc interpolation is used:

$$\bar{U}[(k_x(A,B),0,\omega(A,B)] = \frac{4\pi^2}{\Delta\omega\,\Delta k_x}\sum_m\sum_n \bar{U}(n\Delta k_x, 0, m\Delta\omega) \cdot \frac{\sin\left(\frac{k_x-n\Delta k_x}{\Delta k_x}\right)}{\frac{k_x-n\Delta k_x}{\Delta k_x}} \cdot \frac{\sin\left(\frac{\omega-m\Delta\omega}{\Delta\omega}\right)}{\frac{\omega-m\Delta\omega}{\Delta\omega}}. \tag{19}$$

In the examples discussed later, five grid lines, with both variable m and variable n and closest to the point (k_x, ω), are included in the evaluation of Eq. (19).

The quality of the migrated result depends critically on the sampling intervals ΔA and ΔB, i.e. on the estimates of the length and the depth of the migrated section in Eq. (17). We assume $\bar{U}(k_x, 0, \omega)$ is sampled sufficiently finely by $\Delta k_x=\frac{2\pi}{L}$ and $\Delta\omega=\frac{2\pi}{T}$, such that Eq. (19) is accurate enough for points between the grid points. The nonequally spaced (k_x, ω) points, which contribute to $\bar{M}(A, B)$, may represent a grid which is coarser than the original grid of $\bar{U}(k_x, 0, \omega)$, such that essential features in this spectrum may be lost, and in particular if $\bar{U}(k_x, 0, \omega)$ is a rapidly oscillating function. Then it may happen that pronounced spatial aliasing is produced in the migrated section $M(x, z)$. In such cases, ΔA and ΔB have to be reduced, i.e. X and Z have to be enlarged by increasing LA and LB in Eq. (18). Common practice, however, is to reduce $\Delta\omega$ and Δk_x, i.e. T and L will be increased; because of the assumed relations $X=L$ and $Z=vT$, the result is the same. Increasing T and L is equivalent to adding zeros at the end of the seismograms and zero traces at the end of the geophone array (Stolt, 1978). The disadvantage, however, is that zero traces unnecessarily have to be Fourier transformed from the $x-t$ domain to the $k_x-\omega$ domain, leading to an increase in computing time which may be substantial. The increase in computing time can be reduced or even avoided through multiplication of the spectrum $\bar{U}(k_x, 0, \omega)$ by the phase-shift operator $e^{i(\omega t_0 + k_x x_0)}$. This corresponds to the introduction of a new origin (x_0, t_0) in the $x-t$ domain. If this origin is placed at about the centre of the wave field $U(x, 0, t)$, the resulting spectrum $\bar{U}(k_x, 0, \omega)$ is considerably smoother than before and thus larger sampling intervals ΔA and ΔB can be used. After interpolation, the inverse phase shift is applied, such that the old origin is valid again. This method follows a suggestion of Claerbout (1985) and is similar to the spectral smoothing by the use of reduced travel times which is familiar from the theory of synthetic seismograms for layered media.

Applications

Fast plane-wave migration

The plane-wave migration will be tested on the synclinal model shown in Fig. 2. The model consists of two layers with different velocities v and densities ρ, which are separated by a curved interface having a maximum dip of 35°. A seismic line source S_i is located at the surface and gener-

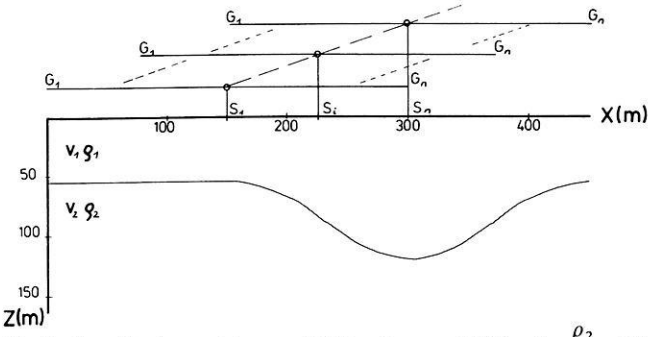

Fig. 2. Synclinal model: $v_1 = 1{,}500$ m/s, $v_2 = 1{,}000$ m/s, $\frac{\rho_2}{\rho_1} = 0.5$. $S_1 \ldots S_n$ denote shotpoints. $G_1 \ldots G_n$ is the geophone spread. The shotpoint-receiver configuration is shifted across the structure in the x direction in order to simulate the field survey

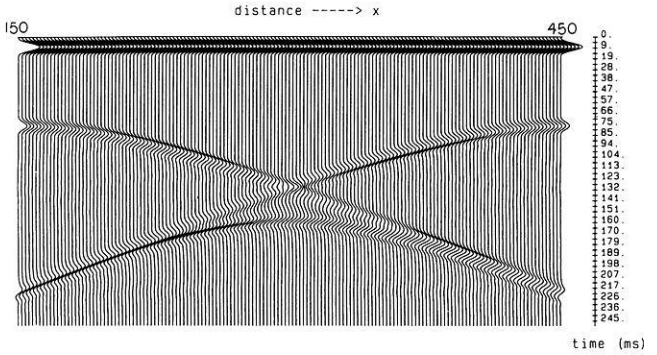

Fig. 3. Plane-wave response of the synclinical model for a plane wave propagating vertically ($\phi = 0$). The direct plane wave starts at time $t = 0$. The reflection is visible between 70 ms and 226 ms

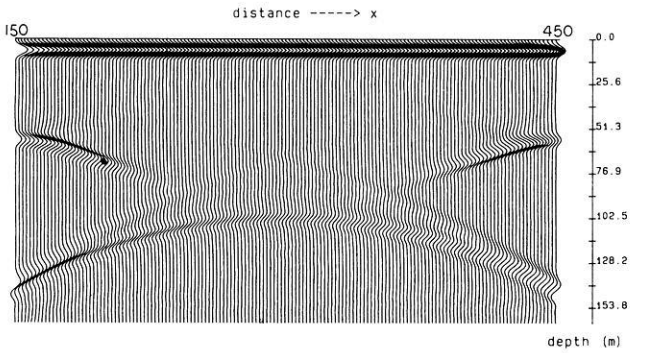

Fig. 4. Frequency-wavenumber migration of the plane-wave response of Fig. 3 without application of the phase-shift operation prior to interpolation. Strong aliased events are visible because of too coarse sampling of $\bar{U}(k_x, 0, \omega)$

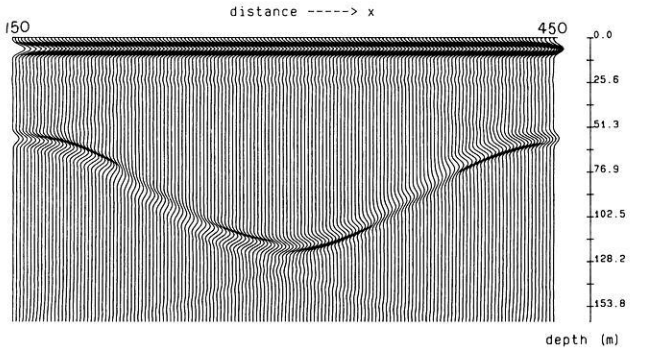

Fig. 5. Improved migrated section of the plane-wave response of Fig. 3, with the phase shift $e^{i(\omega t_0 + k_x x_0)}$ applied prior to interpolation: $t_0 = 113$ ms, $x_0 = 150$ m

ates cylindrical SH waves with a dominant frequency of 50 Hz. The reflection from the syncline is calculated along the finite geophone array $G_1 \ldots G_n$ using a finite-difference technique (Korn and Stöckl, 1982). Reflections coming from the boundaries of the rectangular model are suppressed by using absorbing boundary conditions (Clayton and Engquist, 1980). In order to simulate the field survey, the single-shot experiment is repeated for different shots $S_1 \ldots S_n$ at the surface, shifting the shotpoint-geophone configuration across the structure. The single-shot sections calculated in this way represent the data base for the plane-wave sections which can be synthesized from the single-shot sections by applying the slant-stack technique. The plane-wave sections we will show here have already been used as input data to a finite-difference migration technique (Temme, 1984).

Figure 3 shows the plane-wave response for a plane wave propagating vertically ($\phi = 0$). The geophone array extends from 150 m to 450 m; the section contains 150 seismograms. The sampling interval in time is $\Delta t = 1.89$ ms. For the frequency-wavenumber migration, 106 zero traces have been added on the right side. The number of time samples in each seismogram is $LT = 128$. LA in Eq. (18), i.e. the number of samples along the horizontal wavenumber axis A, has been chosen equal to the number of seismograms $LX = 256$. LB in Eq. (18) has been chosen equal to the number of time samples $LT = 128$. The depth increment $\Delta z = 1.28$ m has been used, and the maximum depth Z of the migrated section is 164 m. The migration result, corresponding to these parameters (Fig. 4), is characterized by strong aliased events; only the upper part of the syncline to a depth of 50 m is migrated correctly. The reason for aliasing is too coarse sampling of $\bar{U}(k_x, 0, \omega)$ in ω. The migrated result can be improved without extra computing time if, prior to migration, a phase shift $e^{i(\omega t_0 + k_x x_0)}$ is applied to the plane-wave section. We have chosen $t_0 = 113$ ms and $x_0 = 150$ m, corresponding to a new origin at the centre of the record section in Fig. 3 (x_0 is measured from the x coordinate of the leftmost seismogram). After migration the phase shift is removed in order to get the true depth structure. The result is shown in Fig. 5. The complete syncline is migrated very well; there is good agreement with the results of the finite-difference migration of Temme (1984, Fig. 6). Segments of the structure lying horizontally, or having small dips, show large amplitudes because the plane wave is vertically incident.

The next example (Fig. 6) shows the slant-stacked section for a plane wave incident under the angle $\phi = -30°$. The plane wave comes in from the right, travels to the left in the negative x direction, and hits upon the left flank of the syncline almost normally. The right side of the traveltime loop, carrying information about the left part of the syncline, is complete; whereas the left side shows a large gap. This is a consequence of the finite geophone spread used in the single-shot experiments. The geophone array again extends from 150 m to 450 m and the plane-wave section contains 150 seismograms. The sampling interval is $\Delta t = 1.89$ ms. For migration, again 106 traces have been added on the right side, so that the total number of seismograms is $LX = 256$. The number of time samples of each seismogram is $LT = 256$ in this experiment. As in the first

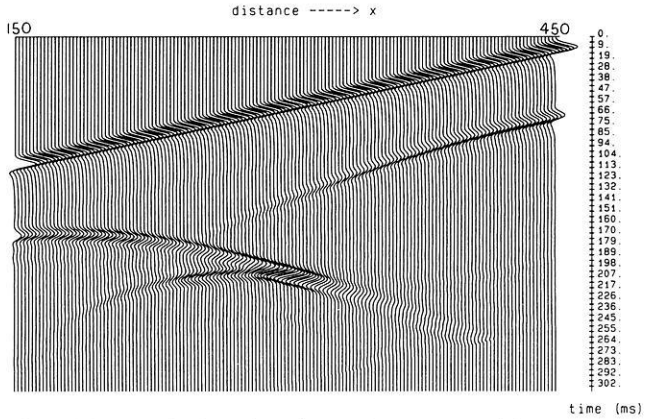

Fig. 6. Slant-stacked section for a plane wave with propagation angle $\phi = -30°$. The plane wave is incident from the right and starts at $t = 0$ at $x = 450$ m; it travels to the left, in negative x direction. The reflection from the syncline is visible between 60 and 260 ms

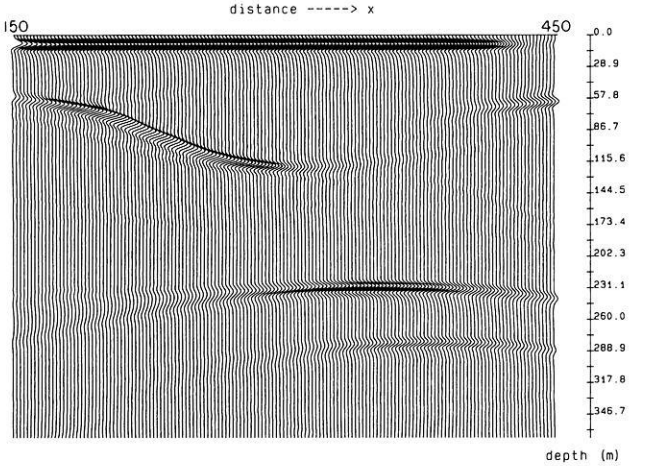

Fig. 7. Migration of the slant-stacked section of Fig. 6 without application of a phase shift. The left-hand part of the structure is successfully reconstructed. Strong aliased events occur at depths of 230–280 m

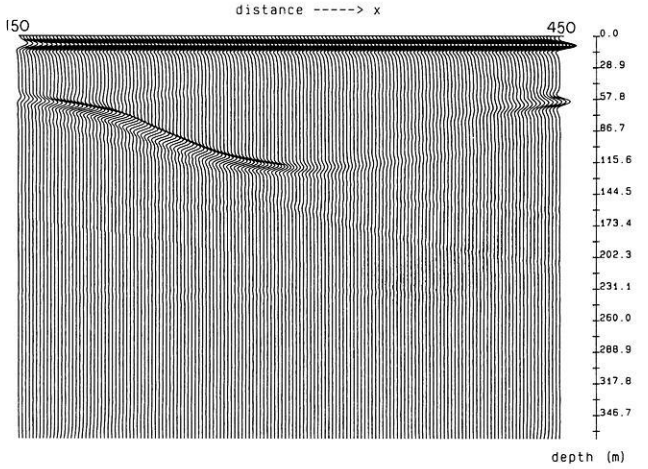

Fig. 8. Improved migrated section of the slant-stacked section of Fig. 6 with application of a phase shift: $t_0 = 132$ ms, $x_0 = 150$ m

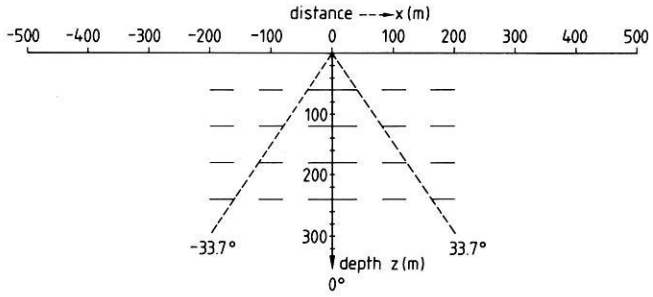

Fig. 9. Twenty horizontal reflectors embedded in a medium of constant velocity and density. For the calculation of *SH* reflections and diffractions, a reflection coefficient has been used which is characterized by a velocity contrast from $v_1 = 1{,}500$ m/s to $v_2 = 1{,}000$ m/s and a density contrast from $\rho_1 = 2$ g/cm^3 to $\rho_2 = 1$ g/cm^3. The line source is located at $(x = 0, z = 0)$

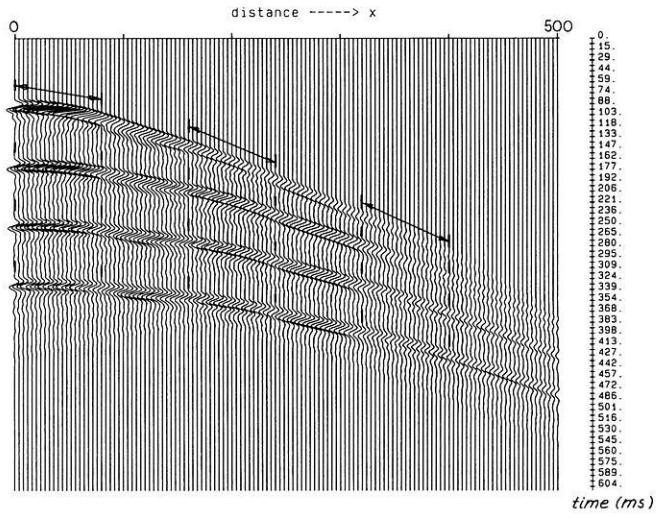

Fig. 10. Synthetic single-shot seismograms calculated along half the geophone array of Fig. 9 from $x = 0$ to $x = 500$ m. The position of each reflection is marked

plane-wave experiment, $LA = LX$ and $LB = LT$ has been chosen and $\Delta z = 1.44$ m has been used.

Figure 7 shows the migrated depth section without application of a phase shift. Again, strong aliased events are present at depths around 230–280 m. Using a phase shift with $t_0 = 132$ ms and $x_0 = 150$ m, we obtain the improved migrated result shown in Fig. 8. As expected, the largest amplitudes occur in the steep dip range of the syncline, where the plane wave comes in vertically. Again there is good agreement with the finite-difference migration results of Temme (1984, Fig. 7).

Fast single-shot migration

For the single-shot migration, the model shown in Fig. 9 was chosen. The structure consists of 20 horizontal reflector elements, which are separated from each other by roughly one wavelength. The shotpoint is located at $x = 0$. The geophone array extends from $x = -500$ m to $x = +500$ m. The synthetic *SH* seismograms for this simple reflector model were calculated with a fast analytical technique (Fertig and Müller, 1979) which is comparable to the finite-difference technique as far as accuracy is concerned. The analytical formula is based on a generalization of the exact theory

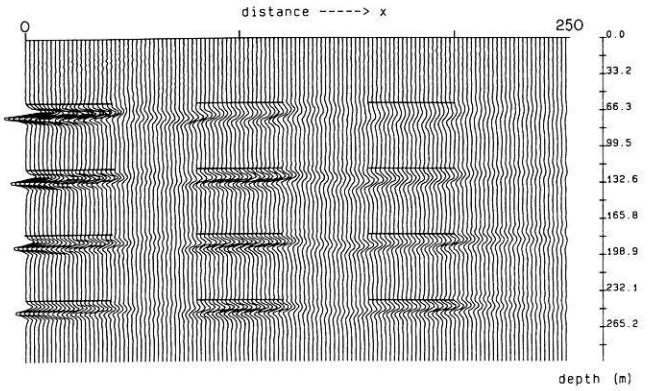

Fig. 11. 45° finite-difference migration of the single-shot section of Fig. 10. The true reflector positions are marked by *thin lines*

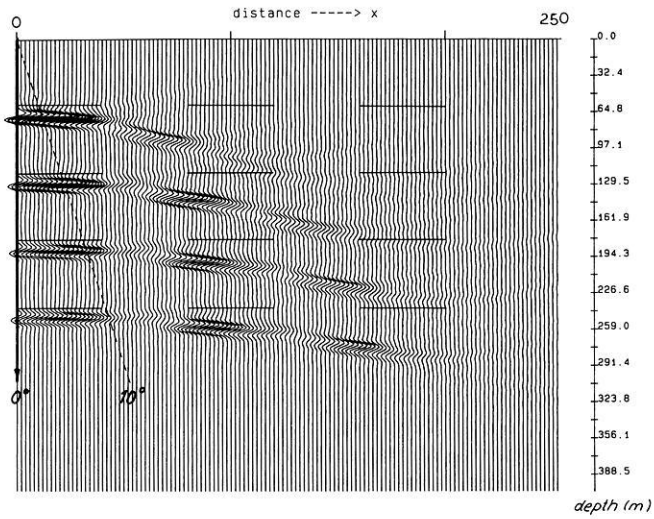

Fig. 12. Fast frequency-wavenumber migration of the single-shot section of Fig. 10 for the sounding direction $\phi = 0$. The ray angle $\phi = 10°$ is shown for orientation. True reflector positions are marked by *thin lines*

for diffraction at an opaque half-plane. Interaction of the reflecting elements with each other cannot be taken into account with this forward modelling technique. The model in Fig. 9 was chosen to demonstrate the effects due to the approximate nature of the imaging condition Eq. (14). As was shown in the derivation of the theory of single-shot migration, the migrated result will be correct only along a specified ray. Here, three rays are investigated. The $-33.7°$ and the $+33.7°$ rays traverse the structure diagonally. We expect the diagonal elements to be migrated more or less correctly. The 0° sounding should give a good image of the elements below $x = 0$.

Figure 10 shows the synthetic seismograms along half the geophone array from $x = 0$ to $x = 500$ m. The position of each reflection is marked along the four hyperbola-like events. Reflections at large x have small amplitudes due to cylindrical spreading and the angle-dependent reflection coefficient. Between the reflections, diffractions from the numerous reflector edges can be seen.

We first show in Fig. 11 the migrated section calculated with the 45° finite-difference technique. This method allows the application of the correct single-shot imaging condition

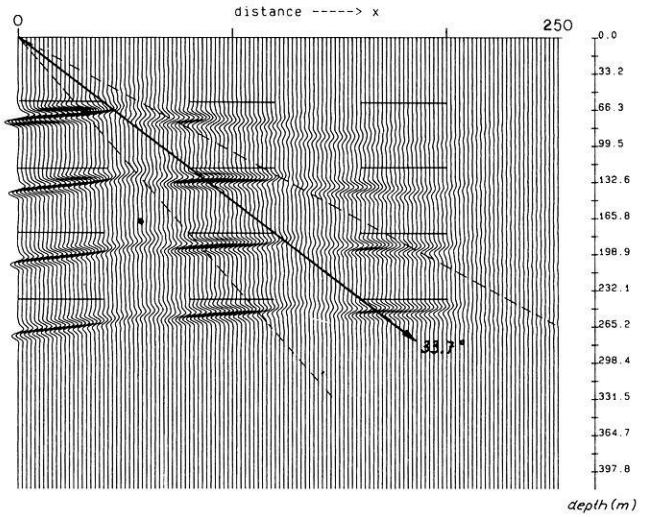

Fig. 13. Fast frequency-wavenumber migration of the single-shot section of the model of Fig. 9 for the sounding direction $\phi = +33.7°$. Ray angles $\phi = 33.7° \pm 10°$ are shown for orientation

Eq. (2); the results serve as a reference for the following fast frequency-wavenumber migrations. We notice in Fig. 11 the good agreement of the reconstructed elements with the true positions indicated by thin lines. Reflections from the upper-right elements propagate with angles of 55°–75° to the surface. For these angles, the 45° approximation of the wave equation becomes inaccurate. As a consequence we see distorted reflectors in the upper-right part of the reconstruction. Reflectors far from the shotpoint show small amplitudes due to cylindrical spreading. Additionally, amplitude variations can be seen along each element, which are caused by the angle-dependent reflection coefficient. Between the reflectors, diffracted energy is focussed to a range of approximately one wavelength.

Figure 12 shows the frequency-wavenumber migration for $\phi = 0°$. A phase shift of $t_0 = 300$ ms and $x_0 = 0$ has been applied. The imaging condition is exact along a ray pointing vertically downwards at $x = 0$. We expect to migrate reflection points at $(x = 0, z)$ correctly. From Fig. 12 we see that also segments within an aperture of 0°–10° are also reconstructed very well. Reflecting elements beyond this range are mispositioned. They are too deep and are shifted towards smaller x values. Comparison of the reconstructed elements with the true reflector positions shows that the error is in the range 0–2 wavelengths.

The same data set was used to reconstruct elements along the sounding direction $\phi = 33.7°$. Figure 13 shows that in this experiment elements lining up diagonally can be reconstructed very well. Additionally, the ray angles $\phi = 33.7° \pm 10°$ are marked for orientation. Reflectors outside this range, again, are mispositioned and show incompletely focussed diffractions.

The entire migrated section, now for the sounding direction $\phi = -33.7°$, is shown in Fig. 14. The array of this example extends from $x = -500$ m to $x = +500$ m. Along the sounding ray the elements are reconstructed very well. We realize for positive x values, however, that the error increases. This is due to the slowness of the exact imaging hyperbola, Eq. (2), changing sign beyond $x = 0$; whereas for the linear approximation, Eq. (14), the slowness remains constant over x.

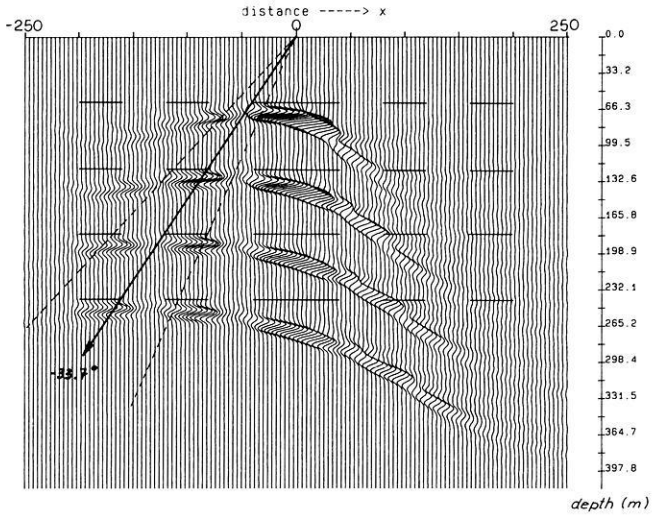

Fig. 14. Fast frequency-wavenumber migration of the entire single-shot section of the model of Fig. 9 for the sounding direction $\phi = -33.7°$

The fast frequency-wavenumber technique needed a computing time for the section in Fig. 12 or 13, which was only 5% of the computing time of the finite-difference technique. Most of the CPU time was used to perform the two-dimensional FFT.

Discussion

Migration of plane-wave and single-shot sections can be performed very fast in the frequency-wavenumber domain. The steps included in this technique, outlined above in detail, are the following. First, the wave field which has been recorded at the earth's surface has to be transformed from the $t-x$ domain to the $\omega-k_x$ domain by using a two-dimensional FFT. In a second step, the spectrum $\bar{U}(k_x, 0, \omega)$ has to be mapped onto a new grid in the $A-B$ wavenumber domain. This is done by prescribing equidistant wavenumbers A, B within the shaded area of Fig. 1 (right panel) and solving Eqs. (10) and (11) for k_x and ω. Usually k_x and ω do not fall on gridpoints in the $\omega-k_x$ domain, and $\bar{U}[k_x(A, B), 0, \omega(A, B)]$ has to be interpolated. The examples shown in this paper have been calculated with a two-dimensional sinc interpolation of order 5, Eq. (19), which is sufficiently good. Tests with linear interpolation were not successful; this simpler interpolation generates background noise all over the migrated section. More critical than the interpolation is the choice of the sampling intervals ΔA and ΔB in Eq. (17). As Figs. 4 and 7 show, large ΔA and ΔB result in strong ghost events in the migrated section. The sampling intervals Δk_x and $\Delta\omega$ are sufficient for representation of the spectrum $\bar{U}(k_x, 0, \omega)$, but the sampling intervals resulting from Eqs. (10) and (11) may be too large, such that details of the spectrum may be lost in the $A-B$ domain. In such cases, a remedy is the phase-shift operation $e^{i(\omega t_0 + k_x x_0)}$ prior to interpolation which smoothes the spectrum. The point $(x = x_0, t = t_0)$ is chosen at about the centre of the record section representing the reflected wave field $U(x, 0, t)$. After interpolation, the phase shift is removed through multiplication by $e^{-i(\omega t_0 + k_x x_0)}$ and the spectrum $\bar{M}(A, B)$ of the migrated section $M(x, z)$ follows from Eq. (13). The final step is an inverse two-dimensional FFT.

Plane-wave migration can be performed exactly with the imaging condition Eq. (1). Plane-wave sections for different angles of incidence, which can be synthesized from single-shot sections by slant stacking, can be used for the reconstruction of selected segments of the structure. An advantage of data stacking which forms part of the plane-wave migration procedure is noise reduction. A disadvantage is that a *complete* plane-wave response is only obtained if the single shots used have a sufficient spread length. Current recording techniques appear to allow the synthesis only for propagation directions close to vertical.

The reconstruction of the subsurface structure from single-shot sections can be performed with the algorithm that has been developed for plane-wave migration. However, a linear approximation of the exact imaging condition by Eq. (14) has to be used. As a consequence, the migrated result is only correct along a ray with direction ϕ with respect to the vertical axis. In Figs. 12–14 reconstruction is successful within an aperture of $\pm 10°$ around this sounding direction; this aperture is frequency dependent and decreases with increasing frequency. As in plane-wave migration, single-shot sections can be used to reconstruct selected segments of the structure. No stacking is involved in single-shot migration, and the danger that noise is migrated is larger than in plane-wave migration. However, it is conceivable that stacking the migration results of closely neighboured shots, all being obtained for the same sounding direction, will produce noise reduction.

Conclusions

In this paper a fast frequency-wavenumber method for migration of single-shot and plane-wave sections was derived. It has been demonstrated that plane-wave migration can be performed exactly in constant-velocity media. The reconstruction of reflecting elements from single-shot sections can be done exactly only along preselected sounding directions. The direction selective features of plane-wave and single-shot migration can be used to reconstruct selected segments of the subsurface structure which are of special interest. It is conceivable that migrated single-shot sections, corresponding to several neighbouring sounding directions, can be combined into one section with extended validity.

As a technical result, it has been demonstrated that a two-dimensional phase shift in the frequency-wavenumber domain prior to migration can improve the migrated result without extra computing costs. The phase-shift operation is useful since it reduces zero padding of the reflected wave field and makes the proposed migration method even more economic.

The migration technique developed here is a straightforward extension of Stolt's (1978) technique for CMP or zero-offset wave fields. Stolt's method is frequently used in industrial practice, in spite of the limitations due to the constant-velocity assumption. We suggest that, in a similar way, the potential of fast plane-wave and, in particular, single-shot migration in the frequency-wavenumber domain be investigated with the abundant data volumes of the prospecting industry.

Since this paper has been completed, we have been able to generalize the fast frequency-wavenumber migration method for the case of depth-dependent velocity (Müller and Temme, in preparation). The focussing properties that were found here for single-shot migration then become more

pronounced: a migrated CMP or plane-wave section is correct only along a preselected horizontal line (and close to it), and a migrated single-shot section only at a preselected point (and close to it). The algorithm is basically the same as that used in this paper.

Acknowledgements. We profited considerably from Getahun Terefe's versions and improvements of two-dimensional FFT programs. The study was funded by a grant from the Deutsche Forschungsgemeinschaft Te 123/1-1. The computations were done at the computing center of the Department of Geology and Geophysics of the University of Utah in Salt Lake City.

References

Claerbout, J.F.: Imaging the earth's interior. Palo Alto: Blackwell Scientific Publications 1985

Clayton, R.W., Engquist, B.: Absorbing boundary conditions for wave-equation migration. Geophysics **45**, 895–904, 1980

Fertig, J., Müller, G.: Approximate diffraction theory for transparent half planes with application to seismic wave diffraction at coal seams. J. Geophys. **46**, 349–367, 1979

Gazdag, J.: Wave equation migration with the phase-shift method. Geophysics **43**, 1342–1351, 1978

Gazdag, J., Squazzero, P.: Migration of seismic data by phase shift plus interpolation. Geophysics **49**, 124–131, 1984

Korn, M., Stöckl, H.: Reflection and transmission of Love channel waves at coal seam discontinuities computed with a finite difference method. J. Geophys. **50**, 171–176, 1982

Loewenthal, D., Lu, L., Roberson, R., Sherwood, J.: The wave equation applied to migration. Geophys. Prosp. **24**, 380–399, 1976

Mayne, W.H.: Common reflection point horizontal data stacking techniques. Geophysics **27**, 927–938, 1962

Schultz, P.S., Claerbout, J.F.: Velocity estimation and downward continuation by wavefront synthesis. Geophysics **43**, 691–714, 1978

Stolt, R.: Migration by Fourier transform. Geophysics **43**, 23–48, 1978

Temme, P.: A comparison of common-midpoint, single-shot, and plane-wave depth migration. Geophysics **49**, 1896–1907, 1984

Terefe, G.: Tiefenmigration im Frequenz-Wellenzahl-Bereich. Diploma thesis, University of Frankfurt, 1985

Treitel, S., Gutowski, P.R., Wagner, D.E.: Plane-wave decomposition of seismograms. Geophysics **47**, 1375–1401, 1982

Received March 25, 1986; revised June 24, 1986
Accepted June 25, 1986